Supporting Information

Room Temperature High-Efficiency Welding of Ultra-Long Silver Nanowire Network for Flexible Transparent Electrodes

Maomao Yao, [#a] Lulu Zhao, [#b] Chunyu Fan, [#a] Xingbo Han, [a] Zhongbin Wu, [*b] Hengda Sun, [*a] Gang Wang [a] and Ru Xiao [*a]

[a.] *State Key Laboratory for Modification of Chemical Fibers and Polymer Materials, College of Materials Science and Engineering, Donghua University, Shanghai 201620, China.*

[b.] *Frontiers Science Center for Flexible Electronics, Institute of Flexible Electronics, Northwestern Polytechnical University, Xi'an 710072, China*

Email: iamzbwu@nwpu.edu.cn, sunhengda@dhu.edu.cn, xiaoru@dhu.edu.cn

Experimental Section

1. Materials and Testing

Silver nitrate ($AgNO_3$), sodium chloride (NaCl), glutaraldehyde, and 1,2-propanediol (1,2-PG) were commercially purchased from China National Pharmaceutical Group Corporation, with analytical grade purity. Poly(3,4-ethylenedioxythiophene)/poly(styrenesulfonate) (PEDOT:PSS) was purchased from Sigma-Aldrich. Unless otherwise specified, these materials did not undergo further purification processes. Polyvinylpyrrolidone (PVP) with an average molecular weight of 55,000 was obtained from China National Pharmaceutical Group Corporation. The drugs involved in the OLED device evaporation included: N,N'-Bis(naphthalen-1-yl)-N,N'-bis(phenyl)benzidine (NPB), 4,4',4''-Tris(carbazol-9-yl)triphenylamine (TCTA), 4,7-Diphenyl-1,10-phenanthroline (Bphen), Acetylacetonatobis(2-phenylpyridine)iridium ($Ir(ppy)_2(acac)$), lithium fluoride (LiF), and aluminum (Al).

The Hitachi SU-8010 cold field emission scanning electron microscope (SEM) system was used for morphological characterization of ul-AgNWs and the welded conductive electrode. The Dimension FastScan atomic force microscope (AFM) from Bruker, Germany, was used for roughness testing of ul-AgNWs transparent conductive electrodes. The Talos F200S field emission transmission electron microscope (TEM) from Czech Republic was used for morphological characterization, lattice structure, and elemental analysis of ul-AgNWs. UV-visible absorption measurements were performed using the Lambda 950 UV-Vis-NIR spectrophotometer (PerkinElmer). Infrared spectra were recorded using the Nicolet iS50 Fourier transform near-infrared spectrometer (Thermo Fisher). The microstructure of suspended and settled particles in the synthesized products was examined using the DVM6 digital video microscope (Leica). The crystal structure was analyzed using the D2 Phaser powder X-ray diffractometer from Bruker AXS, Germany. The mechanical properties of the conductive electrode were tested using a custom-built room temperature bending apparatus. The sheet resistance of the thin films was measured using a four-probe system, with at least 10 positions sampled for each sample to obtain the average value. OLED devices were fabricated using the QHV-R96 OLED vacuum coating equipment from Shenyang Qihui Optoelectronic Technology Co., Ltd. The performance of OLED devices was

characterized using a computer-controlled source meter (Keithley 2450) and a custom-built optical detection system for OLED display panels.

2. Preparation of ul-AgNWs

A 15 mL solution of 0.02 mol/L silver nitrate, 5 mL solution of 0.4 mol/L glutaraldehyde, and 5 mL solution of 1.8 mol/L polyvinylpyrrolidone (K30) were mixed at room temperature and vigorously stirred for 30 minutes. A 15 mL solution of 0.04 mol/L sodium chloride was then added dropwise to the above mixture at a rate of 0.5 mL/min. During the addition, the solution gradually turned milky white, indicating the formation of silver chloride particles. After the addition was complete, the solution was transferred to a 100 mL hydrothermal reaction vessel and placed in an oven pre-set at 160°C for 24 hours. After the reaction, the hydrothermal reaction vessel was removed from the oven and allowed to cool naturally to room temperature to obtain the reaction product. The upper layer of the reaction product was extracted, washed with water and ethanol to remove impurities adhering to the surface of the silver nanowires, resulting in ul-AgNWs with an average length of 317.66 ± 98.60 μm, an average diameter of 78.06 ± 13.87 nm, a maximum length-to-diameter ratio exceeding 6000, and minimal particle content.

3. Preparation and Welding of FTEs

The prepared ul-AgNWs ethanol dispersion was sprayed onto a PET substrate covered with a mask to form a film of overlapping ul-AgNWs, and the welding solution was uniformly sprayed onto the film surface. The welding solution, prepared by mixing a 3 mmol/L silver nitrate aqueous solution with 1,2-PG in a volume ratio of 3:7, was left on the film at 28°C for 2 hours. Subsequently, the film was placed in a 1,2-PG solution and reduced at 60°C for 3 hours, then cooled to room temperature, rinsed with distilled water, and dried in an oven to obtain the welded film.

4. Fabrication of OLEDs

To ensure good electrode testing, the probe area was coated with room temperature curing silver paste. PEDOT:PSS was used as the hole injection layer, spin-coated on the ul-AgNWs electrode, with spin speeds of 1500 r/min, and annealed for 10 minutes at 150°C. The treated electrode was transferred to a vacuum chamber with a vacuum level below 5×10^{-4}, and organic and metal materials were deposited using the OLED vacuum coating equipment. The OLED consisted of the following materials: a 150 nm thick NPB as the hole transport layer; a 10 nm thick TCTA as the electron blocking layer; an emitting layer composed of 10 nm thick TCTA/$Ir(ppy)_2(acac)$ and 10 nm thick Bphen/$Ir(ppy)_2(acac)$, with evaporation rates of 9:1 for TCTA and $Ir(ppy)_2(acac)$, and 9:1 for Bphen and $Ir(ppy)_2(acac)$; a 50 nm thick Bphen as the electron transport layer; a 1 nm thick lithium fluoride (LiF) as the electron injection layer; and a 120 nm thick aluminum (Al) as the cathode.

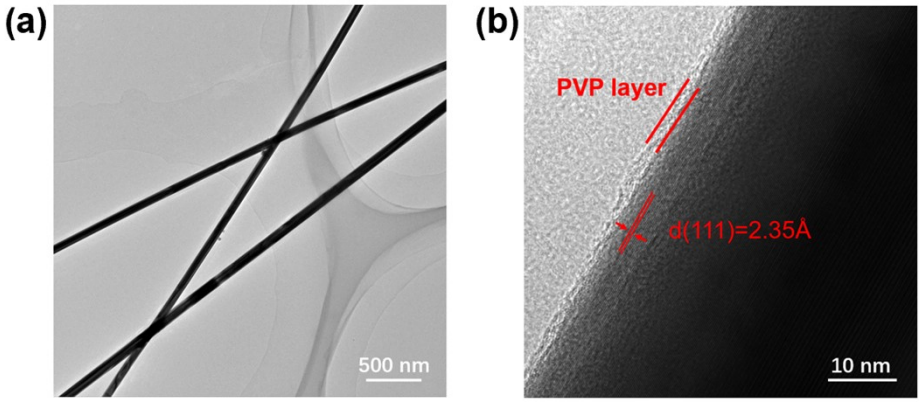

Fig. S1 TEM characterization of ul-AgNWs. (a) Morphology of ul-AgNWs under TEM. (b) Microscopic characterization of ul-AgNWs.

As shown in Fig. S1(a), the ul-AgNWs exhibit a uniform morphology without any defect features. For Fig. S1(b), we measured the lattice spacing of ul-AgNWs to be 2.35 Å, and the observed periodic structure clearly corresponds to the [111] direction of single-crystal silver, highlighting its highly ordered crystal structure.

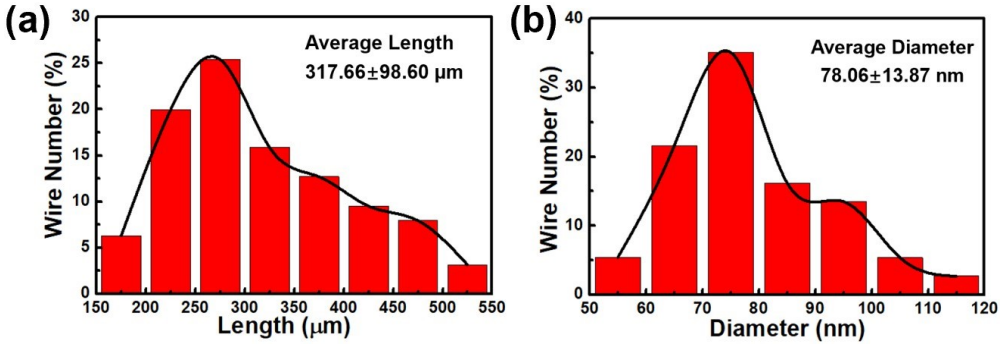

Fig. S2 Histogram of the length (a) and diameter (b) statistical distribution of ul-AgNWs.

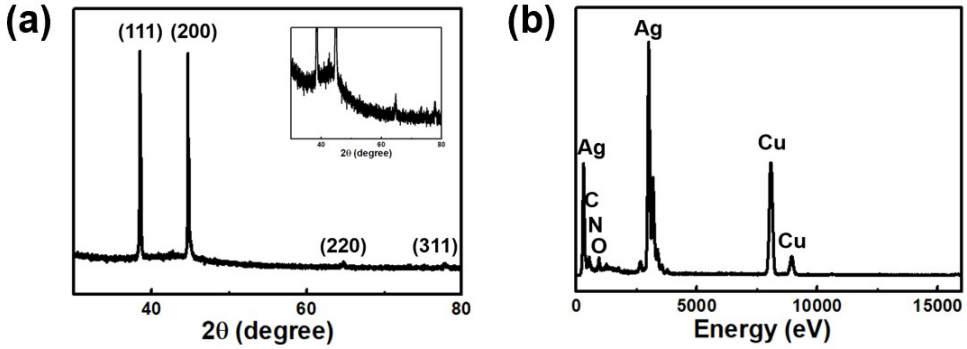

Fig. S3 Spectral characterization of ul-AgNWs. (a) X-ray diffraction pattern (XRD), with an inset showing a magnified view. (b) Analysis and characterization of the elemental composition of ul-AgNWs using an energy dispersive spectrometer (EDS).

We characterized ul-AgNWs using XRD, with the positions of the four diffraction peaks matching those in the standard spectrum (JCPDS no.03-0931), indicating a high degree of cubic

symmetry in the structure of ul-AgNWs. In the EDS, the characteristic peaks of silver clearly indicate the presence of abundant silver elements in the sample, while the influence of PVP as a coating layer on the sample surface is clearly evident in the spectrum.

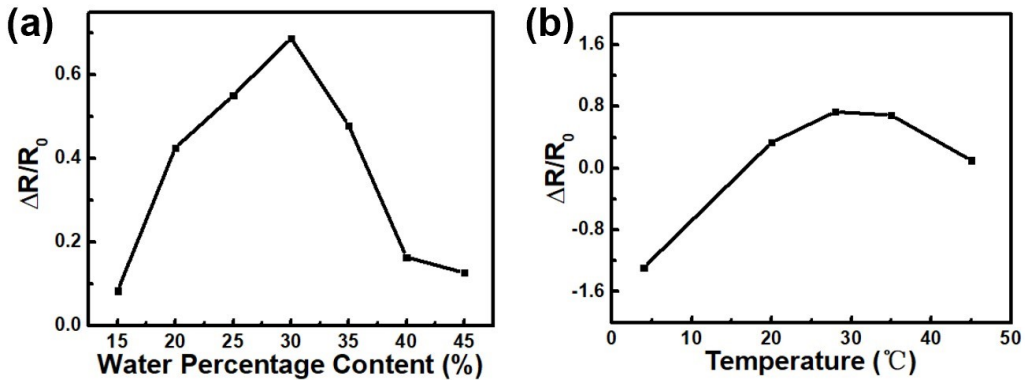

Fig. S4 The influence of the composition ratio of two solvents (a) and the welding temperature (b) on the welding behavior of ul-AgNWs FTEs.

Through the optimization experiments on the impact of the composition ratio of the two solvents and the environmental temperature on the welding behavior, we can deduce that the optimal volume ratio of $AgNO_3$ solution to 1,2-PG is 3:7 and the optimal welding temperature is 28°C. As the surface tension of 1,2-PG is lower than that of water, the mixed solution droplets show both an outward "traction" on the sides of the droplets to flatten them on the surface of the silver nanowires and a tendency to retract due to the liquid's own surface tension. The combined effect of these two forces results in a thin liquid film on both sides of the droplets on the nanowire surface. The liquid content of the film is relatively low and the surface area is large. Due to the easier evaporation of water compared to 1,2-PG, the evaporative effect on the film is more pronounced at an appropriate temperature, resulting in lower water content on the sides of the droplets than in the middle, leading to a reduced surface tension compared to the middle portion. This difference in forces causes the droplets to move along the nanowires. When reaching the intersection of the nanowires, the droplets aggregate due to spatial hindrance and complete the enrichment of the solder.

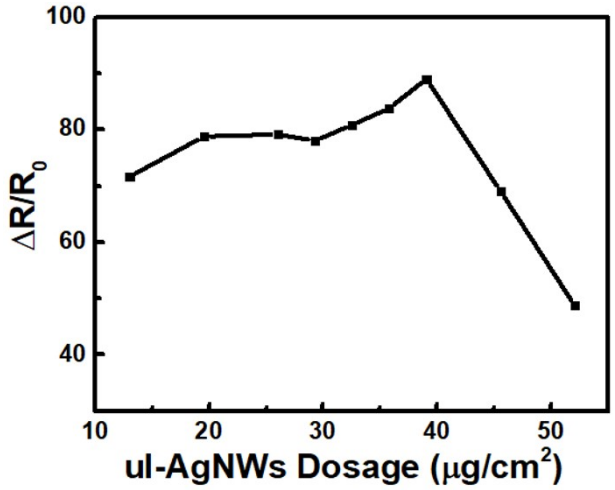

Fig. S5 The trend of the change in sheet resistance of FTEs before and after welding. ΔR refers to the change in sheet resistance value before and after welding, and R_0 refers to the sheet resistance value before welding.

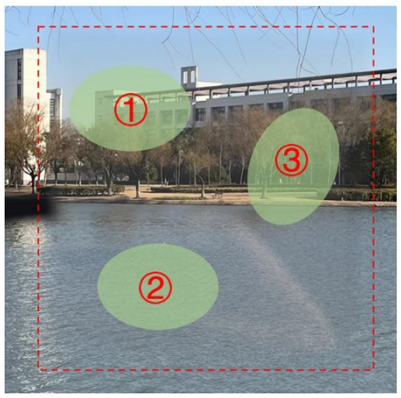

BW: Before Welding
AW: After Welding

Number		①	②	③
T (%)	BW	97.0	97.0	97.1
	AW	98.2	98.1	98.4

Fig. S6 Optical uniformity before and after welding.

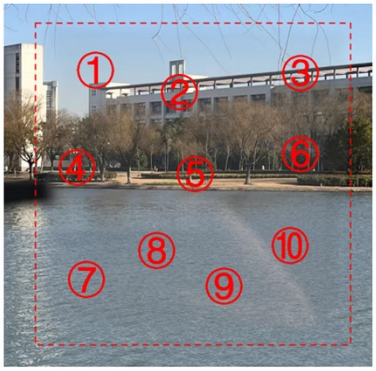

BW: Before Welding
AW: After Welding

Number		①	②	③	④	⑤	⑥	⑦	⑧	⑨	⑩
R (Ω)	BW	603	452	549	732	431	667	503	496	622	556
	AW	55	53	72	56	67	61	50	73	64	63

Fig. S7 Uniformity of electrical properties before and after welding.

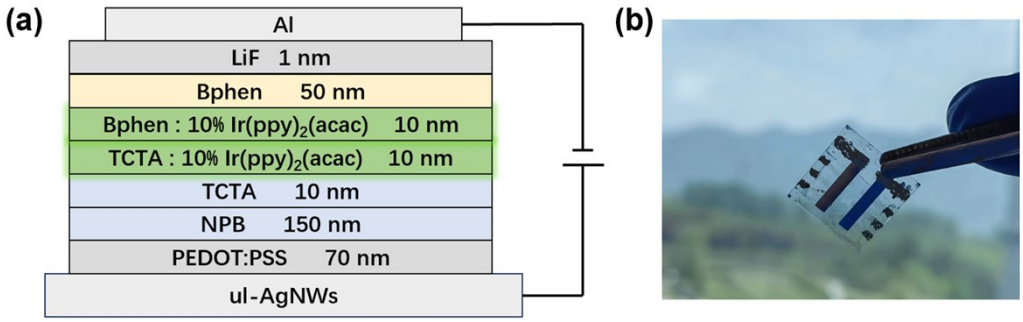

Fig. S8 Structure (a) and physical image (b) of the OLED device.

The FTEs serves as the anode of the OLED device, with PEDOT:PSS and NPB serving as the hole injection and transport layers, TCTA, $Ir(ppy)_2(acac)$, and Bphen serving as the emitting layer, and LiF and Bphen serving as the electron injection and transport layers, with Al serving as the cathode. The specific structure is ul-AgNWs/PEDOT:PSS (70nm)/NPB (150nm)/TCTA (10nm)/TCTA:10wt%$Ir(ppy)_2(acac)$ (10nm)/Bphen:10 wt% $Ir(ppy)_2(acac)$ (10nm)/Bphen (50nm)/LiF (1nm)/Al.

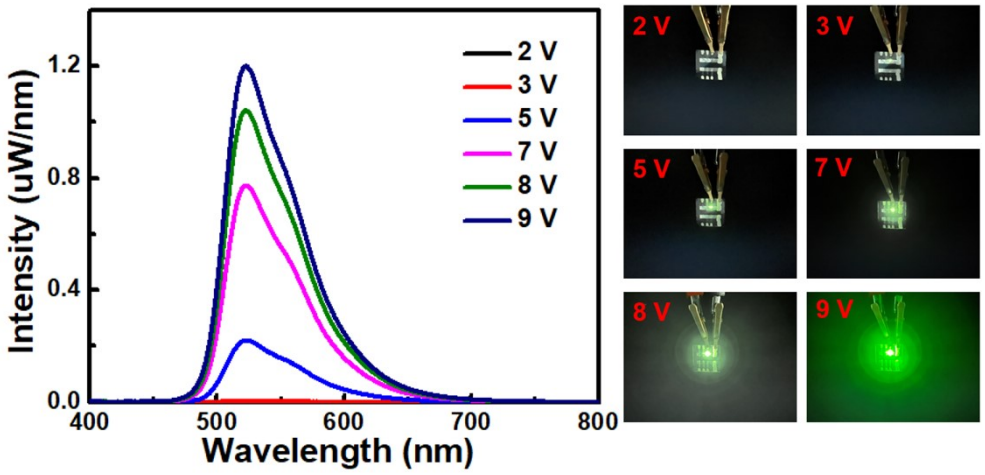

Fig. S9 Luminous intensity of OLEDs at different voltages.

We applied different voltages to the devices made after welding, and the electroluminescence peak of the device was at 522 nm. It can be clearly observed from the spectral data and visually that the OLED's luminous intensity gradually increases with increasing voltage.

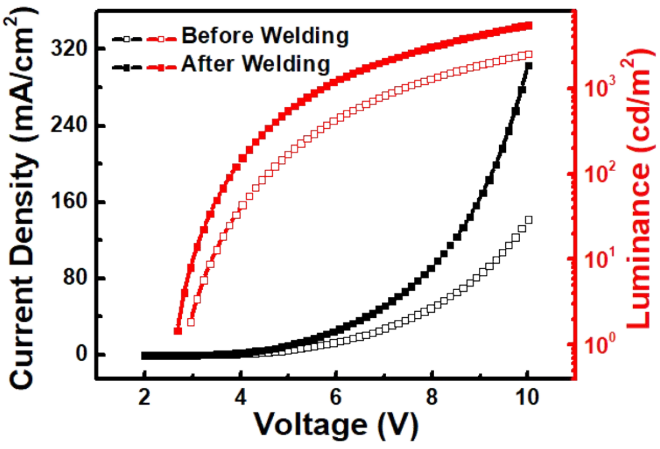

Fig. S10 The current density-voltage-luminance curve of the OLED device.

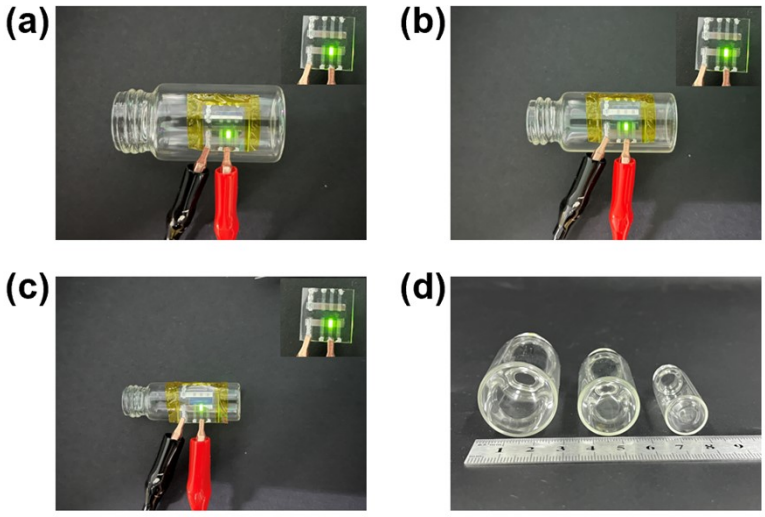

Fig. S11 Luminous performance of OLEDs at different bending angles. (a)-(c) Correspond to bending radii of 13.5 mm, 10.5 mm, and 7.5 mm, respectively. The inset shows the brightness of the device before bending. (d) Side view of the bent surface.